




## Article

# Polyelectrolyte-Surfactant Mixture Effects on Bulk Properties and Antibacterial, Cytotoxic Activity of Fine Sulfur Particles

Seitzhan Turganbay<sup>1,2,\*</sup>, Saule Aidarova<sup>1</sup>, Assem Issayeva<sup>1</sup>, Zhanar Iskakbayeva<sup>2</sup>, Aitugan Sabitov<sup>3</sup>, Gulsinay Turganbay<sup>4</sup> and Alpamys A. Babayev<sup>1</sup>

<sup>1</sup> “One Belt, One Road” Petroleum Engineering Institute, Kazakh-British Technical University, 050000 Almaty, Kazakhstan; s.aidarova@kbtu.kz (S.A.); isa-aseem@mail.ru (A.I.); a\_babayev@mail.ru (A.A.B.)

<sup>2</sup> Microbiology Laboratory, JSC Scientific Center for Anti-Infectious Drugs, 050060 Almaty, Kazakhstan

<sup>3</sup> Nanobiotechnology Laboratory, Combustion Problems Institute, 050012 Almaty, Kazakhstan

<sup>4</sup> Agronomy, Breeding and Biotechnology Institute, Kazakh National Agrarian University, 050010 Almaty, Kazakhstan

\* Correspondence: turganbay.s@gmail.com; Tel.: +7-708-164-47-83

**Abstract:** Elemental sulfur, commonly known for its wide range of biological activities, has a long history of use in protecting all garden and vegetable crops from a range of pests and diseases, including powdery mildew, ascochyta blight, clubroot, plant mites, oidium, anthracnose, and scab. In the present study, a quick and environmentally friendly approach has been developed for the synthesis of sulfur nanoparticles with antibacterial activity. Fine sulfur particles (FSPs) were prepared by modifying the surface of elemental sulfur using various polyelectrolyte–surfactant mixtures (PSMs) including sodium carboxymethyl cellulose–sodium dodecylbenzene sulfonate (NaCMC–SDBS) and polyhexamethylene guanidine hydrochloride–cetyltrimethylammonium bromide (PHMG–CTAB). The FSPs were characterized by UV–visible spectrophotometry, X-ray diffraction (XRD), thermogravimetric/differential scanning calorimetry analysis (TG/DSC), and scanning electron microscopy (SEM), with the FSPs showing an almost spherical shape with an average size in the range of 150–200 nm. The antibacterial activity of the FSPs was tested against Gram-positive *Staphylococcus aureus* and *Enterococcus faecium* and Gram-negative *Escherichia coli* and *Pseudomonas aeruginosa* bacteria and one fungus (*Aspergillus brasiliensis* ATCC 95 16404). Based on this, it could be seen that FSPs exhibited significant antimicrobial activity against Gram-positive bacteria, i.e., *S. aureus* and *E. faecium*. The in vitro cytotoxicity of the FSPs-1 and FSPs-2 studied in normal (MeT-5A) and tumorous (MCF-7) human cell lines was assessed in the concentration range from 500 µg/mL to 0.12 mg/mL, from which it was determined as being non-cytotoxic. The received products can be considered for potential application in agriculture and medicine.

**Keywords:** carboxymethyl cellulose; nanoparticles; sulfur surface; surfactant; elemental; sulfur



**Citation:** Turganbay, S.; Aidarova, S.; Issayeva, A.; Iskakbayeva, Z.; Sabitov, A.; Turganbay, G.; Babayev, A.A. Polyelectrolyte-Surfactant Mixture Effects on Bulk Properties and Antibacterial, Cytotoxic Activity of Fine Sulfur Particles. *Colloids Interfaces* **2024**, *8*, 65. <https://doi.org/10.3390/colloids8060065>

Academic Editor: Wuge Briscoe

Received: 11 June 2024

Revised: 11 October 2024

Accepted: 1 November 2024

Published: 28 November 2024



**Copyright:** © 2024 by the authors. Licensee MDPI, Basel, Switzerland. This article is an open access article distributed under the terms and conditions of the Creative Commons Attribution (CC BY) license (<https://creativecommons.org/licenses/by/4.0/>).

## 1. Introduction

Element sulfur is naturally a pale yellow, insoluble, odorless, and brittle solid, which is chemically and biologically active and which has accordingly seen extensive application in the field of agriculture to combat various kind of mites (ixodid mites, scabies, chicken mites, spider mites), lice, bedbugs, fleas, etc. [1].

However, sulfur has been employed in various forms in contemporary times for crop protection and has been recognized as safe for this purpose [2–4]. It is a significant element in the promotion of plant growth and is synthesized naturally in several plants as a part of their defense against pathogenic infections and invasions [5,6]. In spite of soil supplementation, low-dimensional sulfur particles have shown considerable antimicrobial potential with regard to various fungal (*F. solani*, *V. inaequalis*, *A. brasiliensis*, *C. utilis*, etc.) and bacterial (*P. aeruginosa*, *S. aureus*, etc.) species and show considerable

promise for use as a broad-spectrum pesticide [7,8]. Furthermore, field resistance to elemental sulfur has not been reported, as it has multimodal action that targets multiple sites in phytopathogens [7,9]. Active research focused on the development of new materials based on sulfur nanoparticles with anti-infectious properties is a particular area of study in the modern science of nanodispersed materials. A number of different methods of synthesis of sulfur nanoparticles have been reported in the literature, such as electrochemical methods [10], water–oil microemulsion [11,12], eggshell membrane templating [13], heating sublimed sulfur and polyethylene glycol-200 [14], chemical precipitation [15], the supersaturated solvent method [16], the surfactant-assisted route [17,18], liquid phase precipitation [19], H<sub>2</sub>S reduction by iron chelates in W/O microemulsion [20], and ultrasonic treatment of sulfur-cystine solution [21]. These methods have many disadvantages due to difficulties in scaling up such processes, separation and purification of nanoparticles from the microemulsion, having multistage synthetic processes, and the use of various inorganic and organic acids which requires multiple treatments and which could potentially incur significant harm to human health when using poisonous gases such as hydrogen sulfide.

Polyelectrolytes (PELs), surfactants, and their mixtures are ubiquitous in nature and technology due to their unique properties and versatile functionality. This combination offers synergistic effects that enhance performance in different formulations [22]. When combined, surfactants and polymers can enhance each other's performance and indeed provide additional benefits; for instance, surfactants can improve the dispersibility of the particles, while polymers can contribute to the stability and rheological properties of the suspension. Such combinations are often used in formulations such as emulsions, gels, coatings, and flocculants. Overall, the synergy between surfactants and polymers offers a wide range of applications and benefits, making them valuable components in many industrial and consumer products [23].

Nanoparticles, defined as particles with dimensions in the nanometer scale, have garnered significant attention due to their unique physical, chemical, and biological properties, which differ markedly from their bulk counterparts. Their potential applications span various fields, including medicine, electronics, environmental science, and materials engineering.

Recent advances in nanoparticle research are extensively covered in the review article "Nanoparticles: From Synthesis to Applications and Beyond", published in *Advances in Colloid and Interface Science* (May 2022, Volume 303, 1–12). This comprehensive review provides an in-depth analysis of contemporary methods for synthesizing nanoparticles, emphasizing the importance of modifying particle size, shape, and surface characteristics to achieve desired functionalities. It explores various synthesis techniques, including chemical vapor deposition, sol-gel processes, and biological methods, highlighting the advancements in each approach.

The novelty of this work lies in the use of polyelectrolyte–surfactant mixtures (NaCMC-SDBS and PHMG-CTAB) for the synthesis of FSPs, which has not been widely explored. Additionally, the antibacterial activity and non-cytotoxic nature of these nanoparticles suggest potential applications in agriculture and medicine, highlighting the significance of this study.

Advancing from foundational work, our study focuses on the influence of PSMs on the size and stability of FSPs. We investigate how different concentrations of polyelectrolytes, when added to a surfactant at its optimal concentration, affect the properties of sulfur particles. By integrating recent advancements and exploring specific interactions in our synthesis approach, we aim to contribute to the ongoing development and optimization of nanoparticle systems for various applications. A method for obtaining FSPs through mechanical and ultrasonic grinding is presented. FSPs were obtained by modifying the surface of sulfur with various PSMs, including NaCMC-SDBS (FSPs-1) and PHMG-CTAB (FSPs-2). The synthesized FSPs were characterized using various analytical techniques. The antibacterial activities of the synthesized FSPs were assessed using different cell lines, and the *in vitro* cytotoxicity of the studied FSPs-1 and FSPs-2 against normal (MeT-5A) and

tumor (MCF-7) human cell lines was evaluated in the concentration range of 500 µg/mL to 0.12 mg/mL.

The novelty of this work lies in the use of PSMs (NaCMC-SDBS and PHMG-CTAB) for the synthesis of FSPs, which has not been widely explored. Previous studies have demonstrated that polyelectrolytes and surfactants can significantly enhance the stability and dispersibility of nanoparticles, leading to improved performance in various formulations [24,25]. Additionally, the antibacterial activity and non-cytotoxic nature of these nanoparticles suggest potential applications in agriculture, and the use of sulfur nanoparticles as a broad-spectrum pesticide could offer significant advantages over traditional chemical pesticides given their low toxicity and ability to target multiple sites within phytopathogens, reducing the likelihood of resistance development [26]. Recent research indicates that sulfur nanoparticles can effectively control fungal pathogens like *Fusarium solani* and *Verticillium inaequalis*, which are responsible for substantial crop losses [27].

In the medical field, the antibacterial properties of FSPs open avenues for their use in wound healing and infection control, especially in the context of antibiotic resistance. Studies have shown that sulfur nanoparticles exhibit significant antibacterial activity against a range of pathogens, including *Staphylococcus aureus* and *Pseudomonas aeruginosa* [28,29]. Their biocompatibility and non-cytotoxic nature make them promising candidates for developing novel therapeutic agents that can mitigate infections without adversely affecting human cells [30].

In summary, this study not only advances the understanding of polyelectrolyte-surfactant interactions in the synthesis of sulfur nanoparticles but also highlights the potential for these materials in agricultural and medical applications, thus underscoring the significance of our findings.

## 2. Materials and Methods

### 2.1. Materials

Sulfur, molecular weight 32.06 g/mol (98%, GOST 127.1, Tengizchevroil, Atyrau, Kazakhstan), cetyltrimethylammonium bromide (CTAB, MW 364.45 g/mol), and sodium dodecylbenzene sulfonate (SDBS, MW 348.48 g/mol) were purchased from Sigma-Aldrich (St. Louis, MO, USA, ≥99%), whilst sodium carboxymethyl cellulose (NaCMC, 99%, MW 250000) was purchased from Tianjin Heowns Biochem. LLC., (Tian Jin, China), and polyhexamethylene guanidine hydrochloride (PHMG-HCl, MW 533.03 g/mol) from Quzhou Ebright chemicals. Co., Ltd. (Quzhou, China).

### 2.2. Preparation of Sulfur Nanoparticles

Preparation of FSPs was carried out in two stages. In the first stage, 10 g of crystalline sulfur was milled in an Ultra Centrifugal Mill ZM 300 (Retsch, Haan, Germany) for 3 min. The milling was performed at a speed of 20,000 rpm, with the temperature of the mill chamber maintained at approximately 25 °C. The size of the sulfur powder grains was in the range of 5–60 microns. In the second stage, the milled sulfur powders were dispersed into 100 mL of PSM aqueous solution and ultrasonicated (Sonopuls, Bandelin Electronic UW 200, Berlin, Germany) for 10 min at an amplitude of 60%, which corresponded to an energy input of 367 J/cm<sup>3</sup>. On/off pulses of 2/2 s were used to reduce heat generation. The suspension temperature after treatment was about 50 °C. Then, the crushed sulfur was dried in a Christ ALPHA 1-1 LD plus (Osterode am Harz, Germany) freeze dryer at –50 °C to –60 °C under a vacuum of 0.1 mbar for 24 h, and the experiment was replicated three times. After drying, the samples were milled again using the Ultra Centrifugal Mill ZM-300 for 1 min. So, the samples indeed undergo a second milling step after the drying process to achieve the desired particle size and consistency.

### 2.3. Characterization

The surface charge of FSPs was evaluated via zeta potential and particle size using the dynamic light scattering (DLS) method using a Photocor Compact-Z (Fotokor LLC, Moscow,

Russia). The UV–vis electronic absorption patterns of the FSPs were examined in the range of 190–1100 nm using a LAMBDA-35 UV–vis spectrophotometer (PerkinElmer, Shelton, CT, USA) to confirm the formation of FSPs. The thermal stability of the FSPs was evaluated using a TG/DSC (STA 449 F1 Jupiter, NETZSCH, Berline, Germany). About 10 mg of each sample in a standard aluminum pan was heated from room temperature to 600 °C at a heating rate of 10 °C/min under a nitrogen flow rate of 50 cm<sup>3</sup>/min. Derivatives of TG/DSC were determined using the central finite difference method. The X-ray diffraction patterns of FSPs were investigated using an XRD diffractometer (PANalytical X'pert Pro MRD Diffractometer, Amsterdam, The Netherlands). The spectra were recorded using Cu K $\alpha$  radiation (wavelength of 0.1541 nm) and a nickel monochromator operated at a voltage of 40 kV and a current of 40 mA at diffraction angles in the range of  $2\theta = 5\text{--}80^\circ$  at a scanning speed of 0.4°/min. The morphologies, such as size and shape, of the FSPs were evaluated using scanning electron microscopy (SEM). For this purpose, 10  $\mu$ L of FSPs water suspension was applied dropwise onto a carbon-coated copper grid and allowed to dry, the morphological image of which was recorded using a Quanta 3D 200i (FEITM (Amsterdam, The Netherlands)) operated at an accelerating voltage of 30 kV. Elemental analysis of the FSPs was performed using energy-dispersive spectroscopy (EDS) as part of an SEM instrument (Quanta 3D 200i (FEITM)).

#### 2.4. Test Strains

Antimicrobial properties of FSPs were tested against the following microorganisms: Gram-positive bacteria: *S. aureus* (ATCC 6538-P), *E. faecium* (ATCC 700221). Gram-negative bacteria: *E. coli* (ATCC 8739), *P. aeruginosa* (ATCC 9027), *A. baumannii* (ATCC 1790), *K. pneumoniae* (ATCC 10031). Yeasts: *C. albicans* (ATCC 10231), *C. utilis*. Fungus: *A. brasiliensis* (ATCC 16404).

All test strains were obtained from the American Type Culture Collection (ATCC). Stock cultures were maintained at  $-80^\circ\text{C}$  in low-temperature storage. Before conducting the experiments, bacterial test strains were cultivated and passaged twice on Muller–Hinton Agar, while yeasts and fungi were cultivated on Sabouraud Dextrose Agar, according to ATCC guidelines. The bacterial cells were incubated at 37 °C for 18–24 h, yeasts at 24–26 °C for 24–48 h, and fungi at 25 °C for 2–11 days.

#### 2.5. Test System

The cytotoxicity of FSPs assays was evaluated in two different types of human tumor cell lines, MeT-5A and MCF7.

The MeT-5A cell culture consists of SV40-transformed human mesothelial cells. The cells effectively proliferate at a concentration of  $1 \times 10^5$  cells/cm<sup>2</sup>, reaching 100% growth within two to three days of cultivation. The culture medium used is RPMI-1640 medium supplemented with 10% FBS. The MCF7 cell culture is a line of human breast adenocarcinoma. The MCF7 line retains some characteristics of differentiated mammary epithelium, including the ability to process estradiol via cytoplasmic estrogen receptors and express the oncogene WNT7B. These cell lines are intended solely for scientific laboratory research. The cells effectively proliferate at a concentration of  $1 \times 10^5$  cells/cm<sup>2</sup>, reaching 100% growth within two to three days of cultivation. The culture medium is RPMI-1640 medium supplemented with 10% fetal bovine serum. The cells are cultivated under the following conditions: 37 °C, 5% CO<sub>2</sub>, and 95% humidity. Viability after cryopreservation is  $\geq 90\%$  (staining with trypan blue before cultivation). The source of the cell culture is ATCC.

#### 2.6. Antibacterial Activity of FSPs

##### 2.6.1. Preparation of Inoculum

##### Bacterial Inoculum Preparation

The bacterial inoculum was prepared using a direct suspension method. Using a bacteriological loop, similar colonies from a 24 h test culture grown on solid nutrient media were selected and transferred to a test tube containing sterile saline. The mixture

was carefully homogenized, and the optical density was measured. The bacterial cell density was adjusted to 0.5 McFarland units, which corresponds to a cell concentration of approximately  $1.5 \times 10^8$  CFU/mL.

#### Yeast Inoculum Preparation

The yeast inoculum was also prepared using a direct suspension method. Five colonies of a 24 h cultivated test strain, approximately 1 mm in diameter, were taken from the agar medium and suspended in sterile saline. The mixture was vortexed for 15 s, after which the optical density of the cell suspension was measured. The yeast cell density was adjusted to 0.5 McFarland units, which corresponds to a cell concentration of approximately  $1.0\text{--}5.0 \times 10^6$  CFU/mL.

#### Fungi Inoculum Preparation

*Aspergillus* conidial inoculum suspensions were prepared from well-sporulated cultures grown on Sabouraud dextrose agar for 3–7 days, following CLSI guidelines. For this purpose, the test strain was suspended in saline and measured spectrophotometrically at a 530 nm wavelength to achieve approximately 81% transmittance. The inoculum concentration was adjusted to  $10^6$  CFU/mL, corresponding to a turbidity that ranged from 0.4 to 0.7 McFarland standards [31–34].

#### 2.6.2. Procedure of Antimicrobial Testing

The antibacterial and antifungal properties of FSPs were assessed using the agar well diffusion method. The procedure adhered to the standard protocols for disk diffusion assays. Each test strain's inoculum was adjusted to the required cell concentration and spread onto the surface of the test medium, followed by drying at room temperature for approximately 20 min. Next, wells with a diameter of 6 mm were made in the inoculated agar with a sterile cork borer. Into each well, 100  $\mu$ L of the sample (hydrophilic sulfur nanoparticles) was added, with a nanoparticle concentration of 10 mg/mL. Sulfur at the same concentration (10 mg/mL) served as a reference.

All test plates were incubated at 35 °C according to CLSI guidelines. Antimicrobial activity results were recorded by measuring the inhibition zones (in millimeters) after incubation periods of 18–24 h for bacteria, 24–48 h for yeasts, and 3–7 days for fungi.

#### 2.7. Determination of Cytotoxicity of FSPs In Vitro

The investigated FSPs-1 and FSPs-2 were provided at a concentration of 1 mg/mL diluted in dH<sub>2</sub>O. The investigated substances were added once to wells containing cell suspensions of tumor cell lines at the following concentrations: 500.0, 250.0, 125.0, 62.5, 31.25, 15.63, 7.81, 3.91, 1.95, 0.98, 0.49, and 0.24  $\mu$ g/mL. Each dilution was used in triplicate. RPMI-1640 medium was used as a diluent. The duration of exposure of the investigated substances to the tumor cell lines was 48 h in a CO<sub>2</sub> incubator. Cells without the addition of the investigated substances were used as a negative control.

The arithmetic average of the optical density ( $\bar{Y}$ ) for the negative control was calculated via Equation (1):

$$\bar{Y} = \frac{y_1 + \dots + y_n}{n} = \frac{1}{n} \sum_{i=1}^n y_i \quad (1)$$

where  $Y_i$  is the measurement of the optical density (OD) of each object of the group and  $n$  is the number of objects in the group.

The percentage of surviving cells for each repetition of each concentration of the test substance was calculated according to Equation (2):

$$\% \text{ Viability} = \frac{Y_i}{\bar{Y}_{NC}} \times 100\% \quad (2)$$



where  $Y_i$  is the OD measured for each group and  $\bar{Y}_{NC}$  is the arithmetic average OD ( $\bar{Y}$ ) for negative control.

The standard deviation and a percentage of surviving cells were calculated for each test substance as per Equation (3):

$$StD = \sqrt{\sum_{i=1}^n (Y_i - \bar{Y})^2 / (n - 1)} \quad (3)$$

### 2.8. MTT Test

The method for determining the viability of cell cultures is based on the ability of living cells to convert the soluble yellow bromide 3-(4,5-dimethylthiazol-2-yl)-2,5-diphenyl tetrazolium (MTT) into insoluble purple-blue intracellular formazan crystals. Non-viable dead cells do not possess this capability. Four hours before the end of exposure to the tested compounds, a solution of MTT at a concentration of 5 mg/mL was added to the cultured cells. The cells were then incubated for the remaining 4 h in a CO<sub>2</sub> incubator at 37 °C, 5% CO<sub>2</sub>, and 95% humidity. After removing the culture medium, the formazan crystals were dissolved in 100 µL of DMSO for 10 min. The amount of formazan crystals increases in direct proportion to the number of viable cells. The optical density (OD) of the dissolved formazan was measured using a Sunrise RC.4 microplate reader (Tecan Austria GmbH, Salzburg, Austria) at a wavelength of 492 or 540 nm [35].

## 3. Results and Discussion

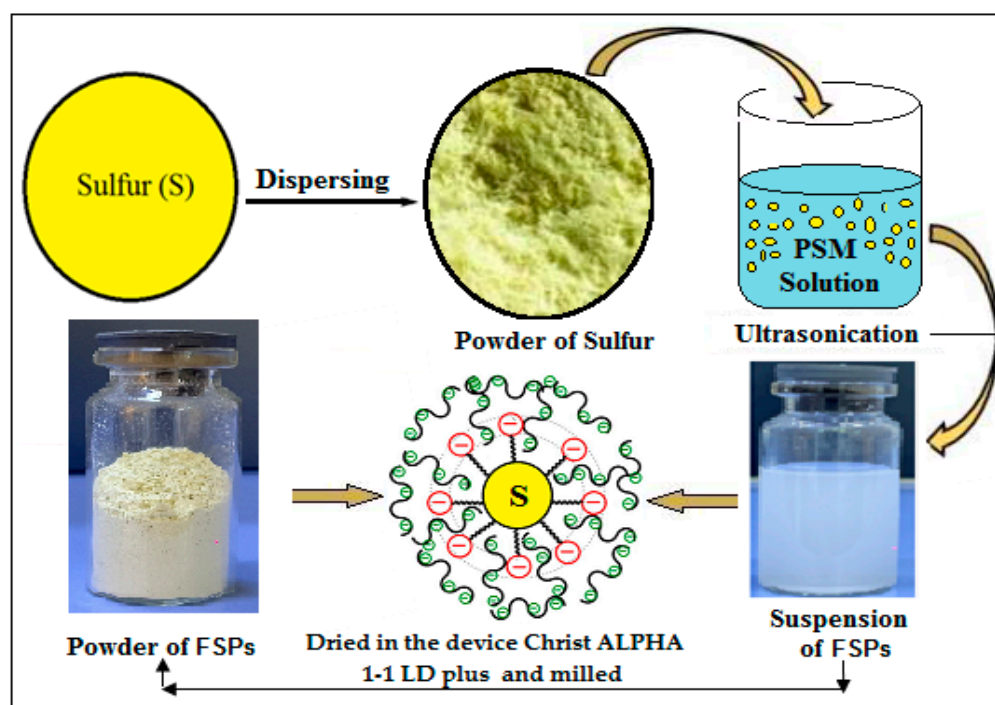
### 3.1. Effect of Surfactants on the Particle Size of Sulfur

It is well known that surfactants capable of adsorbing onto the surface of solid microcrystals reduce the surface tension at the solid/liquid interface and create two-dimensional pressure [36]. This, in turn, weakens intermolecular interactions, reduces aggregate formation, and increases the number of nanoparticles. This phenomenon is a good illustration of the Reh binder effect [37]. We previously investigated the influence of the surfactants CTAB and SDBS on the particle sizes and zeta potentials of FSPs. The results indicated that the optimal surfactant concentrations were 0.36 mM for SDBS and 1.0 mM for CTAB [38].

In this study, we demonstrate how polyelectrolyte–surfactant complexes affect the size and stability of sulfur particles when different concentrations of polyelectrolytes are added to the surfactant (at optimal concentration). For the first time, the effects of adding two mixtures of polyelectrolyte and surfactants, NaCMC-SDBS and PHMG-CTAB, on the size distributions and zeta potentials of FSPs were investigated, the results of which are presented in Table 1. As shown in Table 1, the composition of 0.01% NaCMC-SDBS + Sulfur (FSPs-1) and 0.01% PHMG-CTAB + Sulfur (FSPs-2) represented the optimal polyelectrolyte concentrations in each instance, providing smaller particle sizes of 178 and 175 nm, respectively. The zeta potentials of these particles were approximately −27.28 mV and 38.16 mV, respectively, indicating that in the presence of the NaCMC-SDBS and PHMG-CTAB mixture, first, the polyelectrolytes adsorb onto the surface of the sulfur along with the surfactant, increasing the electrostatic repulsion force and reducing aggregate formation. The stabilization of FSPs is influenced by the effects of PSMs. The Helmholtz–Smoluchowski equation plays a crucial role in explaining the system's stability [39,40]. Although the viscosity values for NaCMC-SDBS and PHMG-CTAB mixtures have not yet been experimentally determined, the stability of the system is directly linked to the zeta potential values. According to the Helmholtz–Smoluchowski equation, the viscosity of the system is strictly proportional to the zeta potential, and increasing these two values leads to decreasing, which, in turn, reduces particle aggregation (coagulation) and enhances stability. This process is depicted in Scheme 1.

**Table 1.** Effects of different concentrations of NaCMC and PHMG polyelectrolytes on sizes and zeta potentials of FSPs.

Surfactant Type	Polyelectrolyte Type	Polyelectrolyte Concentration %	Particle Size (nm)	Zeta Potential (mV)
Anionic SDBS	Anionic NaCMC	0.001	183 ± 6.11	−21.38 ± 0.63
		0.01	178 ± 3.78	−27.28 ± 1.27
		0.1	182 ± 3.52	−31.33 ± 0.33
		0.25	190 ± 3.18	−38.90 ± 1.48
		0.001	188 ± 4.23	28.45 ± 2.07
Cationic CTAB	Cationic PHMG	0.01	175 ± 6.83	38.16 ± 0.42
		0.1	180 ± 4.26	53.00 ± 2.49
		0.25	183 ± 3.71	53.60 ± 2.57

**Scheme 1.** Formation of FSPs.

### 3.2. UV–Visible Spectrophotometry of FSPs

The progress with regard to the formation of FSPs synthesized from various PSMs was monitored using a UV–visible spectrophotometer in the range of 200–800 nm, as shown in Figure 1. The characteristic UV–visible peaks of FSPs-1 and FSPs-2 synthesized from NaCMC-SDBS and PHMG-CTAB were observed at 285 and 280 nm, respectively, indicating the formation of FSPs. Suryavanshi et al. [41] also found the maximum absorption peak of FSPs to be around 290 nm. The appearance of absorption peaks at 223 and 199 nm, characteristic of SDBS and CTAB, respectively, indicated the adsorption of surfactants onto the surface of the sulfur nanoparticles. This confirms the presence of surfactants in the structure of the obtained nanoparticles [42]. The absence of characteristic peaks of polyelectrolytes in the UV spectrum may be due to the low concentration of polyelectrolytes, as well as the presence of surfactants, which can mask the absorption peaks of polyelectrolytes in the UV spectrum [43].

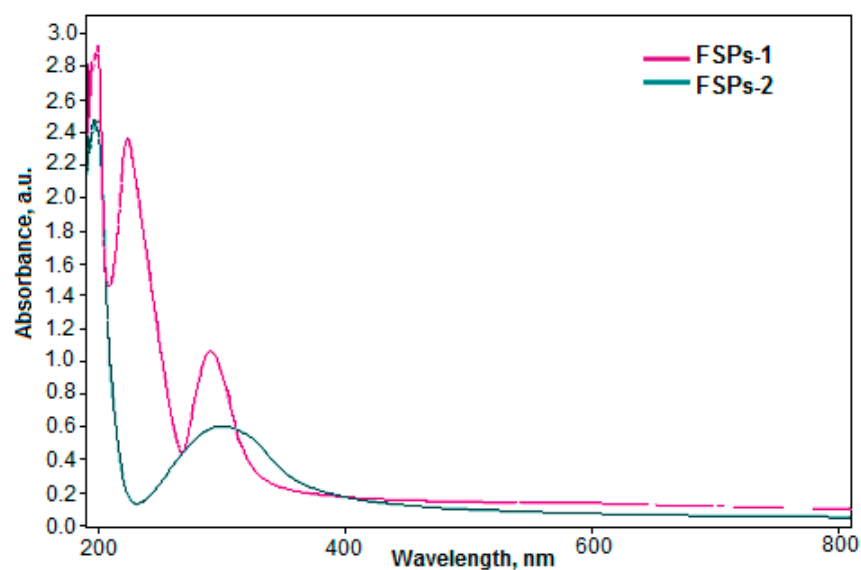


**Figure 1.** UV–visible spectra of FSPs.

### 3.3. Thermal Stability of FSPs

Figure 2 shows the TG/DSC thermograms of the FSPs at heating rates of  $10 \text{ K min}^{-1}$ . In the DSC curve, the endothermic peaks at around  $100$  and  $121$  °C can be, respectively, attributed to the transition of rhombic to monoclinic forms and the solid–liquid transition of FSPs. The endothermic peak at around  $170$  °C can be attributed to the polymerization of FSPs [44]. The endothermic peaks at around  $300$ – $400$  °C can be attributed to the degradation of PSMs, indicative of the presence of a PSM on the surface of the FSP. The endothermic peaks at around  $400$ – $450$  °C can be attributed to the strong volatilization of FSPs. In the TG curves in Figure 2, the obvious mass losses begin at about  $250$  °C, where the vapor pressure of sulfur is  $13 \text{ mm Hg}$ . The mass losses end at  $378$  °C for the curve associated with FSPs-1 and  $385$  °C for the curve associated with FSPs-2. Due to the volatilization of sulfur, 100% mass loss is achieved before its melting point is achieved. The char content after  $400$  °C was between 3.25 and 4.13% of the initial weight, which indicated that the FSPs are thermostable, as their degradation was not complete over the tested temperature range.

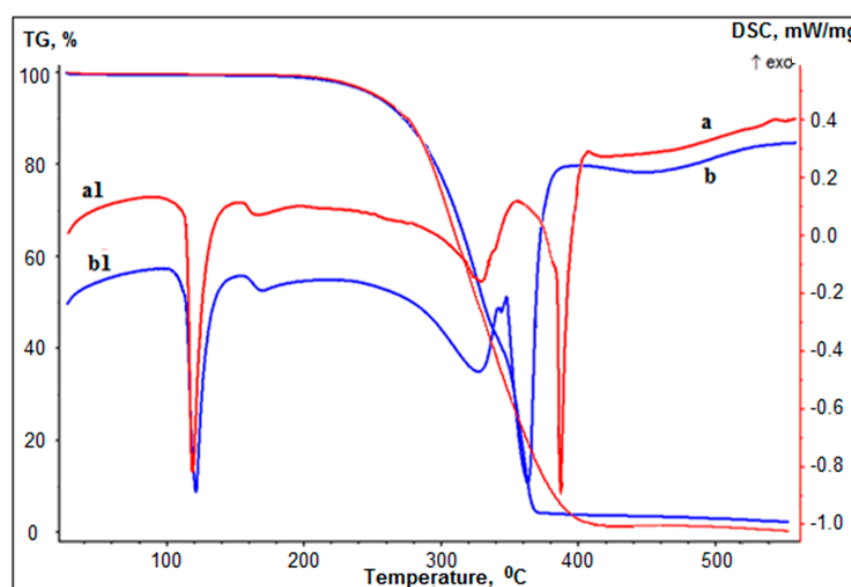


**Figure 2.** TG/DSC thermograms of FSPs. a, a1—TG/DSC of FSPs-1; b, b1—TG/DSC of FSPs-2.



### 3.4. XRD Analysis of FSPs

The XRD analyses of FSPs-1 and FSPs-2, as shown in Figure 3, revealed diffraction peaks corresponding to orthorhombic  $\alpha$ -sulfur with an S8 molecular structure (JCPDS PDF No. 74-1465). Characteristic peaks were observed at  $2\theta$  values of  $21.47^\circ$ ,  $22.18^\circ$ ,  $23.23^\circ$ ,  $23.37^\circ$ ,  $25.19^\circ$ ,  $26.41^\circ$ , and  $27.63^\circ$ , consistent with the literature and reference standards [11]. These results confirm that the synthesized FSPs maintain their crystallographic integrity and match known sulfur phase diffraction patterns.

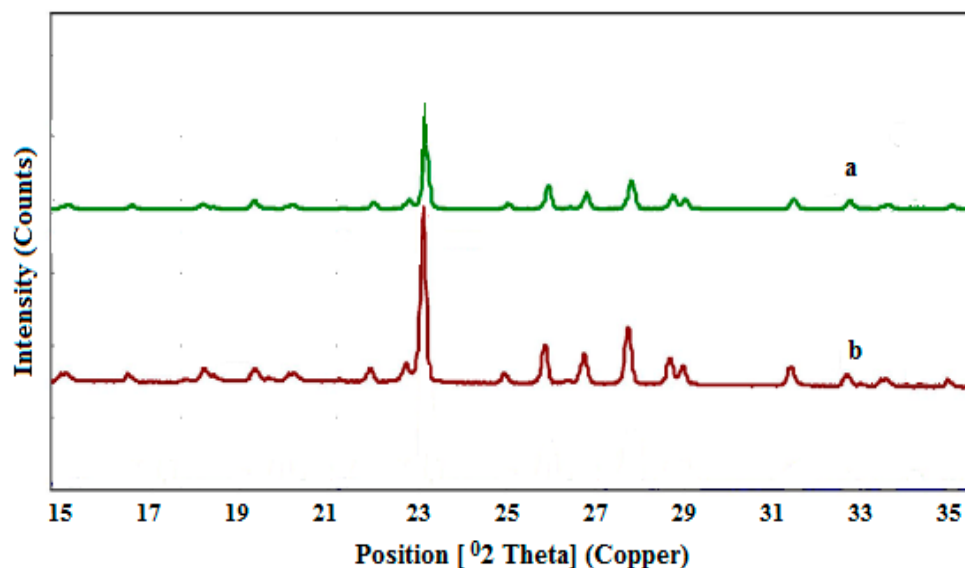
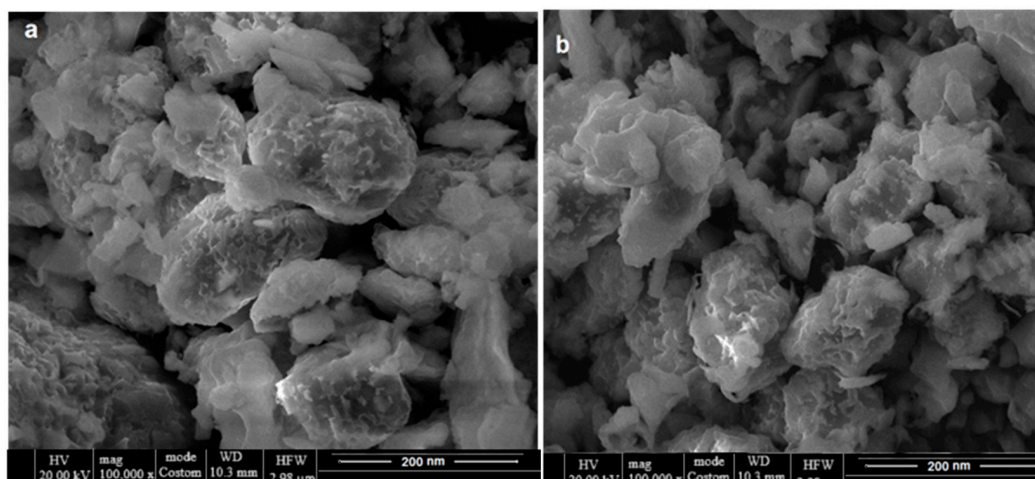


Figure 3. XRD pattern of FSPs: a—FSPs-1, b—FSPs-2.

SDBS typically shows broad diffraction peaks, indicating a semi-crystalline or amorphous nature [45,46]. CTAB, on the other hand, displays distinct crystalline peaks at around  $2\theta$  values of  $21$ – $22^\circ$ , attributed to its lamellar structure [47,48]. NaCMC and PHMG-HCl generally show broad amorphous peaks in the range of  $20$ – $23^\circ$ , reflecting the lack of a well-defined crystalline structure [49,50]. Therefore, when surfactants such as SDBS, CTAB, NaCMC, and PHMG-HCl are used at low concentrations during the synthesis of sulfur nanoparticles, their amorphous nature or low quantity does not significantly affect the dominant sulfur crystalline structure. As a result, distinct diffraction peaks do not appear in the XRD patterns.

### 3.5. SEM Analysis of FSPs

Figure 4 shows the SEM images of FSPs-1 and FSPs-2 (Figure 4a,b). The SEM micrographs showed that FSPs-1 and FSPs-2 were granular to ellipsoidal in irregular shape with smooth surfaces, with the addition of either NaCMC-SDBS or PHMG-CTAB. The morphologies of FSPs have previously been investigated by Dop R.A. et al. [51], who found that they exhibited an ellipsoidal morphology with a mean diameter of  $30\ \mu\text{m}$ . The particle size of the FSPs observed in the SEM images was consistent with the results obtained from DLS experiments. The accumulation of small particles could be what led to the formation of large particles, the size of which ranged from  $150$  to  $200\ \text{nm}$ . The SEM images confirmed the influence of the polyelectrolyte–surfactant in terms of decreasing the size of the FSPs. Interestingly, there was no significant difference in the effect of cationic or anionic surfactants on their ultimate shape.



**Figure 4.** SEM micrographs of FSPs. (a)-FSPs-1, (b)-FSPs-2.

### 3.6. Elemental Analysis of FSPs

The atomic contents of the FSPs-1 and FSPs-2 were confirmed by EDX, the results of which are presented in Figure 5. The EDX spectra of FSPs-1 and FSPs-2 show peaks around 2.4 keV, confirming the purity of the FSPs. The studied samples contain 89.64% and 88.09% sulfur, low intensity 2.78% and 4.20% carbon. 3.77% and 8.85% oxygen peaks were found, indicating the capping of PSMs NaCMC-SDBS and PHMG-CTAB on the surface of FSPs. The absence of any other signal indicated that the prepared FSPs were of a high degree of purity.

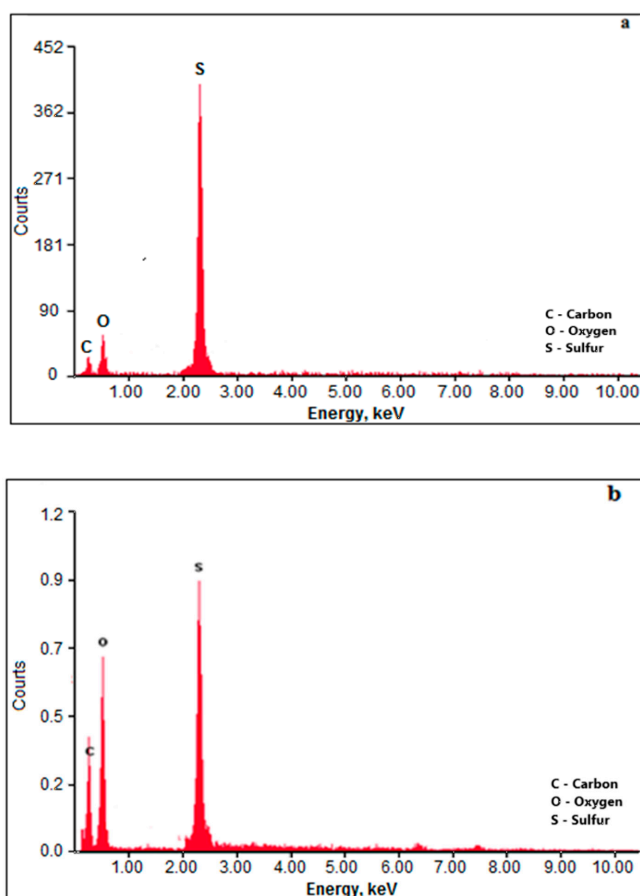


**Figure 5.** EDX spectra of FSPs. (a)-FSPs-1, (b)-FSPs-2.

### 3.7. Investigation of the Antimicrobial Potential of FSPs

The antimicrobial properties of FSPs have been assessed in this study. The results revealed that the FSPs particles efficiently suppressed the growth of test strains with variable potencies.

As shown in Table 2 (Figures S1–S3), sulfur particles FSPs-1 and FSPs-2 exhibited antimicrobial activity while pure PHMG-CTAB, NaCMC-SDBS mixtures and the control powder of sulfur samples did not show growth exhibition for all test strains taken into the experiment.

**Table 2.** Antimicrobial activities of FSPs.

Microorganism	Zone of Inhibition, M ± StD, mm (According to CLSI)				
	FSPs-1	NaCMC-SDBS	FSPs-2	PHMG-CTAB	Sulfur
Gram negatives					
<i>E. coli</i> ATCC 8739	6.0 ± 0.0	6.0 ± 0.0	22.3 ± 0.58	6.0 ± 0.0	6.0 ± 0.0
<i>P. aeruginosa</i> ATCC 9027	6.0 ± 0.0	6.0 ± 0.0	6.0 ± 0.0	6.0 ± 0.0	6.0 ± 0.0
<i>A. baumannii</i> ATCC 1790	6.0 ± 0.0	6.0 ± 0.0	17.3 ± 2.3	6.0 ± 0.0	6.0 ± 0.0
<i>K. pneumoniae</i> ATCC 10031	6.0 ± 0.0	6.0 ± 0.0	18.0 ± 0.0	6.0 ± 0.0	6.0 ± 0.0
Gram positives					
<i>S. aureus</i> ATCC 6538-P	20.0 ± 0.0	6.0 ± 0.0	17.7 ± 0.58	6.0 ± 0.0	6.0 ± 0.0
<i>E. faecium</i> ATCC 700221	19.7 ± 0.58	6.0 ± 0.0	21.7 ± 1.15	6.0 ± 0.0	6.0 ± 0.0
Yeasts					
<i>C. albicans</i> ATCC 10231	7.3 ± 0.58	6.0 ± 0.0	30.7 ± 0.58	6.0 ± 0.0	6.0 ± 0.0
<i>C. utilis</i>	6.0 ± 0.0		51.3 ± 1.15	6.0 ± 0.0	6.0 ± 0.0
Fungi					
<i>A. brasiliensis</i> ATCC 16404	14.7 ± 0.58	6.0 ± 0.0	35.3 ± 0.58	6.0 ± 0.0	6.0 ± 0.0

Note: meanings  $\leq 6.0 \pm 0.0$  indicates the absence of antimicrobial activity.

We detect antimicrobial activity of FSPs-1 against Gram positives *S. aureus* ATCC 6538-P with inhibition zone  $20.0 \pm 0.0$  mm and *E. faecium* ATCC 700221 with inhibition zone  $19.7 \pm 0.58$  mm, respectively. Moreover, the sample showed a zone of inhibition for the yeast *C. albicans* ATCC 10231 of  $7.3 \pm 0.58$  mm. The antifungal effect of FSPs-1 was showed against *A. brasiliensis* ATCC 16404, where it managed to have a  $14.7 \pm 0.58$  mm inhibition zone. All the test results of the disk diffusion method indicated that FSPs-1 did not show antibacterial effect against the Gram-negative (*E. coli* ATCC 8739, *P. aeruginosa* ATCC 9027, *A. baumannii* ATCC BAA-1790, *K. pneumoniae* ATCC 10031) bacteria and *Candida utilis* yeasts cells.

The disk diffusion test results for Gram negatives showed that FSPs-2 did not show growth inhibition for *P. aeruginosa* ATCC 9027 but showed significant growth inhibition of *E. coli* ATCC 8739 ( $22.3 \pm 0.58$  mm), *A. baumannii* ATCC BAA-1790 ( $17.3 \pm 2.3$  mm), and *K. pneumoniae* ATCC 10031 ( $18.0 \pm 0.0$  mm) compared the antibacterial activity of FSPs-1.

FSPs-2 formulation showed characteristic antimicrobial activity against *S. aureus* ATCC 6538-P and *E. faecium* ATCC 700221, as shown in Table 2. Growth inhibition zones of *S. aureus* ATCC 6538-P and *E. faecium* ATCC 700221 were  $17.7 \pm 0.58$  mm and  $21.7 \pm 1.15$  mm, respectively. The strongest fungicidal efficacy of SNPs-2 was observed against *C. albicans* ATCC 10231 and *C. utilis*, with inhibition zones of  $30.7 \pm 0.58$  mm and  $51.3 \pm 1.15$  mm, respectively. The growth inhibition zone of *A. brasiliensis* ATCC 16404 was  $35.3 \pm 0.58$  mm.

While the antimicrobial potential of SNPs has been acknowledged, there remains a scarcity of research evaluating their antibacterial effects. Choudhury et al. [4] recently demonstrated that nanosized sulfur exhibited antibacterial properties against both Gram-positive and Gram-negative bacteria, unlike elemental sulfur, which showed no such

inhibition of bacterial growth. Conversely, Suleiman et al. [11] observed significant antibacterial activity of sulfur nanoparticles against the Gram-positive bacterium *S. aureus*, but not against *E. coli*. This can be explained by the fact that Gram-negative bacteria have an outer membrane [52], which creates a barrier that prevents or limits penetration of sulfur nanoparticles into the bacterial cell and may enhance self-aggregation between nanoparticles. In our study, we selected both Gram-positive and Gram-negative bacteria as test organisms and found that FSPs-1 exhibited no inhibitory effect against Gram negatives. FSPs-2, however, exhibited remarkable bactericidal effects against both Gram negatives and Gram positives, demonstrating exceptional antibacterial efficiency. The higher antibacterial activity of FSPs-2 compared to FSPs-1 may be attributed to the cationic surface charge of FSPs-2 due to the polyelectrolyte–surfactant mixtures. This positive charge potentially facilitates binding of FSPs-2 to the negatively charged bacterial cell membrane. Although the precise mechanism of action of FSPs remains unclear, it is theorized that they bind to the bacterial cell wall, leading to membrane rupture, cell lysis and, ultimately, cell death.

### 3.8. Cytotoxic Effects of FSPs In Vitro

The aim of this study was to investigate the in vitro cytotoxicity of the investigated substances FSPs-1 and FSPs-2 against normal (MeT-5A) and tumor (MCF-7) human cell lines. The substances were initially dissolved in distilled water at concentrations of 1 mg/mL, and for cytotoxicity testing, further dilution was performed with a culture medium in a 1:1 ratio. Cytotoxicity was evaluated in the concentration range from 500 µg/mL to 0.12 µg/mL. The quantitative assessment of the cytotoxic effect of the investigated substances was carried out using the MTT assay. The results of the study showed a dose-dependent decrease in the percentage of viable cells relative to the investigated substances, as depicted in Figure 6.

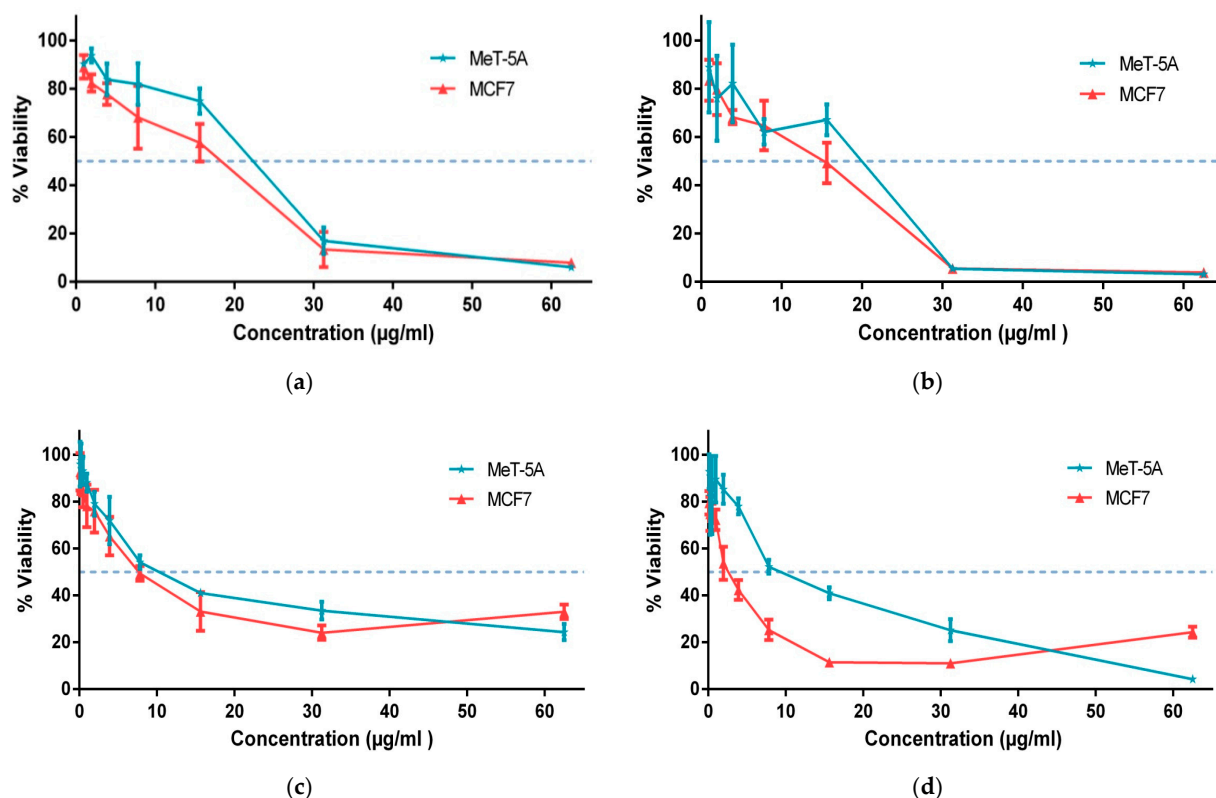


**Figure 6.** Determination of the concentration of the investigated substances at 50% viability (a) Substance FSPs-1 at 24 h exposure, (b) Substance FSPs-1 at 48 h exposure, (c) Substance FSPs-2 at 24 h exposure, (d) Substance FSPs-2 at 48 h exposure.

Table 3 presents the half-maximal inhibitory concentrations ( $IC_{50}$ ) for the investigated substances FSPs-1 and FSPs-2, as well as for the comparator drug, doxorubicin.

**Table 3.** Cytotoxic effects of the investigated substances FSPs-1 and FSPs-2 on normal and tumor human cell lines after 24 and 48 h exposure.

Test Substances	Cytotoxic Concentration $50 \pm StD$ ( $\mu\text{g/mL}$ )			
	24 h		48 h	
	MeT-5A	MCF7	MeT-5A	MCF7
Substance FSPs-1	$20.50 \pm 2.13$	$15.06 \pm 3.08$	$19.16 \pm 3.51$	$14.26 \pm 2.85$
Substance FSPs-2	$5.97 \pm 0.59$	$4.55 \pm 0.62$	$10.66 \pm 0.48$	$3.14 \pm 0.57$
Doxorubicin	NA	$0.087 \pm 0.03$	NA	$0.058 \pm 0.02$

Note: average values from three independent experiments; NA—no activity.

Based on the results obtained, it can be concluded that the investigated substances exhibit cytotoxic effects over a 48-h exposure period. After 48 h of exposure, the  $IC_{50}$  were as follows: for FSPs-1 on MeT-5A,  $19.16 \mu\text{g/mL}$ ; on MCF7,  $4.26 \mu\text{g/mL}$ ; for SNPs-2 on MeT-5A,  $10.66 \mu\text{g/mL}$ ; and on MCF7,  $3.14 \mu\text{g/mL}$ .

A comparative analysis of the  $IC_{50}$ s of the investigated substances, FSPs-1 and FSPs-2, was also conducted (Figure 7).

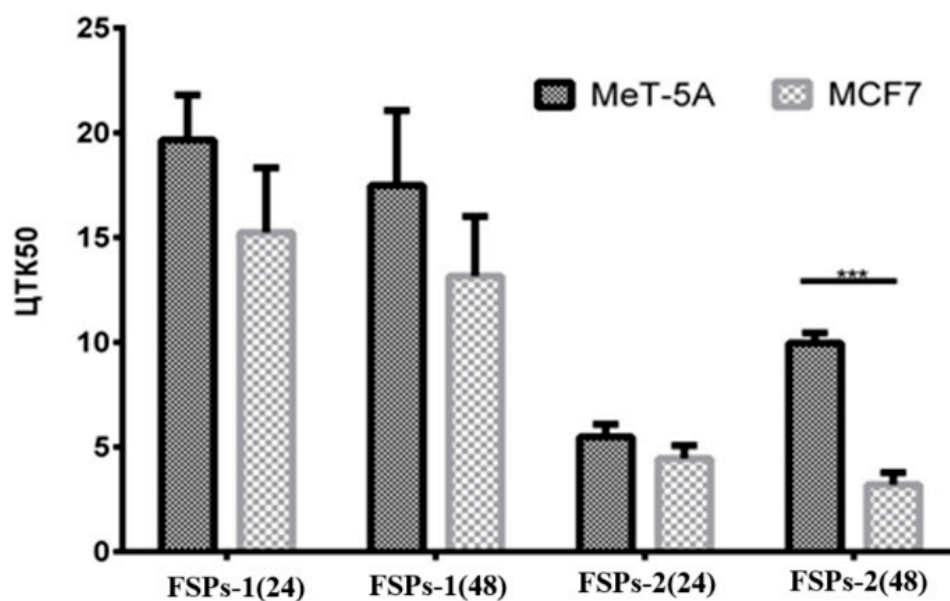


**Figure 7.** Comparative analysis of the effects of the investigated substances on normal and tumor cell lines ( $IC_{50}$ , mean  $\pm$  StD;  $n = 4$ ). Significant differences between groups are indicated by ‘\*\*\*’ ( $p < 0.001$ ).

As evident from the obtained data, the investigated substances, FSPs-1 and FSPs-2, exhibit cytotoxic effects at different concentrations.

Analysis of the cytotoxicity of FSPs-1 showed that the introduction of the solution at concentrations of  $19 \mu\text{g/mL}$  and  $20 \mu\text{g/mL}$  led to moderate cytotoxicity, i.e., resulted in more than 50% cell death in the non-tumor cell line, MeT-5A, and, at concentrations above  $14 \mu\text{g/mL}$ , exhibited moderate cytotoxicity towards the tumor cell line, MCF7. The cytotoxic effect on the tumor cell line showed no significant difference in comparison to the MeT-5A cell line.

Analysis of the cytotoxicity of FSPs-2 showed a cytotoxic effect on the non-tumor cell line, MeT-5A, at concentrations of  $5 \mu\text{g/mL}$ , and on the tumor cell line, MCF7, at concentrations of  $3 \mu\text{g/mL}$  and  $6 \mu\text{g/mL}$ . Remarkably, statistical analysis of FSPs-2 data



showed a significant cytotoxic difference towards the tumor cell line, which is 2.5 times lower than for normal cells.

It was established that FSPs-1 exhibits non-significant selective cytotoxicity towards the human tumor cell line, MCF7, while being minimally toxic towards the normal cell line, MeT-5A.

Summarizing the obtained data, it can be concluded that FSPs-2 possesses significant selective cytotoxicity towards the tumor cell line, MCF7, making this substance highly promising for further investigation.

#### 4. Conclusions

The FSPs synthesized using NaCMC-SDBS and PHMG-CTAB surfactant mixtures demonstrated promising antimicrobial activity, particularly against Gram-positive bacteria, fungi, and yeasts. FSPs-1 showed specific inhibition towards Gram-positive bacteria and fungi, while FSPs-2 displayed broader antimicrobial potential, excluding a few Gram-negative bacteria. These results suggest that FSPs could be developed as antibacterial and fungicidal agents, with particular potential for agricultural and medical applications.

The feasibility of applying these nanoparticles lies in their simple and environmentally friendly synthesis, which makes them suitable for scaling up. However, challenges such as ensuring consistent particle size distribution and stability during large-scale production need to be addressed. Further optimization of the synthesis process could mitigate these issues, enhancing the reproducibility and cost-effectiveness of mass production.

Additionally, while the cytotoxicity studies indicated some selective action against tumor cells, further in-depth studies are required to explore this potential fully. Overall, the FSPs synthesized in this study offer significant potential for practical applications, but further research is necessary to optimize their performance and ensure safe, large-scale use.

**Supplementary Materials:** The following supporting information can be downloaded at: <https://www.mdpi.com/article/10.3390/colloids8060065/s1>, Figure S1: Photographs of zone inhibition on the agar plates; Figure S2: Photographs of zone inhibition on the agar plates; Figure S3: Photographs of zone inhibition on the agar plates.

**Author Contributions:** Conceptualization, S.T. and S.A.; methodology, S.T. and Z.I.; investigation, S.T. and A.I.; formal analysis: G.T. and A.A.B.; writing—original draft preparation, S.T., S.A. and A.S.; writing—review and editing, S.T.; visualization, Z.I. and G.T.; supervision, S.T., A.S. and A.I. All authors have read and agreed to the published version of the manuscript.

**Funding:** This research was funded by grant number AP14972917 “Development of novel highly effective bactericidal and fungicidal sulfur nanoparticles to create anti-infectious agents and ensure biosafety for 2022-2024”, provided by the Ministry of Science and Higher Education of the Republic of Kazakhstan.

**Data Availability Statement:** All the data in this study are included in the manuscript and Supplementary Materials. Enquiries may be made to the corresponding authors.

**Acknowledgments:** The authors would like to thank the control and analytical laboratory, “SCAID”, for assisting in the preparation of the materials for this article.

**Conflicts of Interest:** The authors declare no conflicts of interest.

#### References

1. Chantongsri, A.; Phuektes, P.; Borlace, G.N.; Aiensaard, J. Antifungal activity of green sulfur nanoparticles synthesized using *Catharanthus roseus* extract against *Microsporium canis*. *Thai J. Vet. Med.* **2021**, *51*, 705–713. [CrossRef]
2. Rao, K.J.; Paria, S. Use of sulfur nanoparticles as a green pesticide on *Fusarium solani* and *Venturia inaequalis* phytopathogens. *RSC Adv.* **2013**, *3*, 10471–10478. [CrossRef]
3. Awwad, A.M.; Salem, N.M.; Abdeen, A.O. Novel approach for synthesis sulfur (S-NPs) nanoparticles using *Albizia Julibrissin* Fruits Extract. *Adv. Mater. Lett.* **2015**, *6*, 432–435. [CrossRef]
4. Choudhury, S.R.; Ghosh, M.; Mandal, A.; Chakravorty, D.; Pal, M.; Pradhan, S.; Goswami, A. Surface-modified sulfur nanoparticles: An effective antifungal agent against *Aspergillus niger* and *Fusarium oxysporum*. *Appl. Microbiol. Biotechnol.* **2011**, *90*, 733–743. [CrossRef]



5. Inoue, H.; Kawano, G.; Nagasawa, H.; Sakuda, S. Isolation of elemental sulfur as a self-growth-inhibiting substance produced by *Legionella pneumophila*. *Appl. Environ. Microbiol.* **2002**, *68*, 4809–4811.
6. He, H.; Zhang, C.G.; Xia, J.L.; Peng, A.A.; Yang, Y.; Jiang, H.C.; Zheng, L.; Ma, C.Y.; Zhao, Y.D.; Nie, Z.Y.; et al. Investigation of elemental sulfur speciation transformation mediated by *Acidithiobacillus ferrooxidans*. *Curr. Microbiol.* **2009**, *58*, 300–307. [[CrossRef](#)]
7. Shankar, S.; Jaiswal, L.; Rhim, J.W. New insight into sulfur nanoparticles: Synthesis and applications. *Crit. Rev. Environ. Sci. Technol.* **2021**, *51*, 2329–2356. [[CrossRef](#)]
8. Shahab, S.; Mastaneh, S.; Rhim, J.W. Antimicrobial activity of sulfur nanoparticles: Effect of preparation methods. *Arab. J. Chem.* **2020**, *13*, 6580–6588. [[CrossRef](#)]
9. Cooper, R.M.; Williams, J.S. Elemental sulphur as an induced antifungal substance in plant defence. *J. Exp. Bot.* **2004**, *55*, 1947. [[CrossRef](#)]
10. Shamsipur, M.; Pourmortazavi, S.M.; Roushani, M.; Kohsari, I.; Hajimirsadeghi, S.S. Novel approach for electrochemical preparation of sulfur nanoparticles. *Microchim. Acta.* **2011**, *173*, 445–451. [[CrossRef](#)]
11. Soleimani, M.; Aflatouni, F.; Khani, A. A new and simple method for sulfur nanoparticles synthesis. *Colloid. J.* **2013**, *75*, 112–116. [[CrossRef](#)]
12. Guo, Y.; Zhao, J.; Yang, S.; Yu, K.; Wang, Z.; Zhang, H. Preparation and characterization of monoclinic sulfur nanoparticles by water-in-oil microemulsions technique. *Powder Technol.* **2006**, *162*, 83–86. [[CrossRef](#)]
13. Cheng, X.; Cheng, K.; Liu, J.; Sun, X. Synthesis and Characterizations of Nanoparticle Sulfur Using Eggshell Membrane as Template. *Mater. Sci. Technol.* **2011**, *675*, 279–282. [[CrossRef](#)]
14. Xie, X.Y.; Li, L.Y.; Zheng, P.S.; Zheng, W.J.; Bai, Y.; Cheng, T.F.; Liu, J. Facile synthesis, spectral properties and formation mechanism of sulfur nanorods in PEG-200. *Mater. Res. Bull.* **2012**, *47*, 3665. [[CrossRef](#)]
15. Massalimov, I.A.; Shainurova, A.R.; Khusainov, A.N.; Mustafin, A.G. Production of sulfur nanoparticles from aqueous solution of potassium polysulfide. *Russ. J. Appl. Chem.* **2012**, *85*, 1832–1837. [[CrossRef](#)]
16. Wu, H.; Wang, A.; Yin, H.; Zhang, D.; Jiang, T.; Zhang, R.; Liu, Y. Preparation of sulfur sheets by supersaturated solvent method in the presence of organic modifiers. *Mater. Lett.* **2008**, *62*, 1996. [[CrossRef](#)]
17. Chaudhuri, R.G.; Paria, S. Synthesis of sulfur nanoparticles in aqueous surfactant solutions. *J. Colloid. Interface Sci.* **2010**, *343*, 439. [[CrossRef](#)]
18. Chaudhuri, R.G.; Paria, S. Growth kinetics of sulfur nanoparticles in aqueous surfactant solutions. *J. Colloid. Interface Sci.* **2011**, *354*, 563. [[CrossRef](#)]
19. Gokoglu, N. Novel natural food preservatives and applications in seafood preservation: A review. *J. Sci. Food Agric.* **2019**, *99*, 2068–2077. [[CrossRef](#)]
20. Deshpande, A.S.; Khomane, R.B.; Vaidya, B.K.; Joshi, R.M.; Harle, A.S.; Kulkarni, B.D. Sulfur nanoparticles synthesis and characterization from H<sub>2</sub>S gas, using novel biodegradable iron chelates in W/O microemulsion. *Nanoscale Res. Lett.* **2008**, *3*, 221. [[CrossRef](#)]
21. Xie, X.Y.; Zheng, W.-J.; Bai, Y.; Liu, J. Cystine modified nano-sulfur and its spectral properties. *Mater. Lett.* **2009**, *63*, 1374. [[CrossRef](#)]
22. Kogej, K.; Seven, C. Polyelectrolytes and Surfactants in Aqueous Solutions: From Dilute to Concentrated Systems. In *Advances in Planar Lipid Bilayers and Liposomes*; Iglič, A., Ed.; Academic Press: Cambridge, MA, USA, 2012; Volume 16. [[CrossRef](#)]
23. Tulpar, A.; Tilton, R.D.; Walz, J.Y. Synergistic effects of polymers and surfactants on depletion forces. *Langmuir* **2007**, *23*, 4351–4357. [[CrossRef](#)]
24. Fu, C.; Liu, N. Study of the Synergistic Effect of the Nanoparticle-Surfactant-Polymer System on CO<sub>2</sub> Foam Apparent Viscosity and Stability at High Pressure and Temperature. *Energy Fuels.* **2020**, *34*, 13707–13716. [[CrossRef](#)]
25. Mirtič, J.; Paudel, A.; Laggner, P.; Hudoklin, S.; Julijana, K. Polyelectrolyte-surfactant complex nanoparticles as a delivery platform for poorly soluble drugs: A case study of ibuprofen loaded cetylpyridinium-alginate system. *Int. J. Pharm.* **2020**, *580*, 119199.
26. Vasylychenko, A.V.; Derevianko, S. Antifungal activity of a composition of selenium and iodine Nanoparticles. *Acta. Univ. Agric. Et Silv. Mendel. Brun.* **2021**, *69*, 491–500. [[CrossRef](#)]
27. Sadek, M.E.; Shabana, Y.M.; Sayed-Ahmed, K.; Abou Tabl, A.H. Antifungal Activities of Sulfur and Copper Nanoparticles against Cucumber Postharvest Diseases Caused by *Botrytis cinerea* and *Sclerotinia sclerotiorum*. *J. Fungi* **2022**, *8*, 412. [[CrossRef](#)]
28. Hashem, N.M.; Abdelrahman, A.A.; Zakeer, S. Antimicrobial activities encountered by sulfur nanoparticles combating Staphylococcal species harboring scmec A recovered from acne vulgaris. *AIMS Microbiol.* **2021**, *7*, 481–498. [[CrossRef](#)] [[PubMed](#)]
29. Mashkoo, S.; Mahan, N.; Habeeb, K.; Abd, A. Biosynthesis of Sulphur Nanoparticles and discovering its effectiveness for some biological applications. *J. Phys. Conf. Ser.* **2022**, *2322*, 012067.
30. Rai, M.; Ingle, A.P.; Paralikar, P. Sulfur and sulfur nanoparticles as potential antimicrobials: From traditional medicine to nanomedicine. *Expert Rev. Anti-Infect. Ther.* **2016**, *14*, 969–978.
31. Espinel-Ingroff, A.; Fothergill, A.W.; Ghannoum, M.A.; Pfaller, M.A.; Rex, J.H.; Walsh, T.J. *M51-A: Method for Antifungal Disk Diffusion Susceptibility Testing of Nondermatophyte Filamentous Fungi; Approved Guideline*; CLSI: Wayne, PA, USA, 2010; Volume 30, NO. 11.
32. Mandeel, Q.; Taha, A. Assessment of in vitro. *Antifung. Act. Var. Extr. Indig. Bahraini Med. Plants. Pharm. Biol.* **2005**, *43*, 164–172. [[CrossRef](#)]

33. Espinel-Ingroff, A.; Arthington-Skaggs, B.; Iqbal, N.; Ellis, D.; Pfaller, M.A.; Messer, S.; Rinaldi, M.; Fothergill, A.; Gibbs, D.L.; Wang, A. Multicenter Evaluation of a New Disk Agar Diffusion Method for Susceptibility Testing of Filamentous Fungi with Voriconazole, Posaconazole, Itraconazole, Amphotericin B, and Caspofungin. *J. Clin. Microbiol.* **2007**, *45*, 1811–1820. [[CrossRef](#)] [[PubMed](#)]
34. Ioana, A.; Colosi, O.F.; Bérangère, D.; Cécile, B.; Bernadette, L.; Horațiu, A.; Colosi, H.P. Susceptibility of 100 filamentous fungi: Comparison of two diffusion methods, Neo-Sensitabs and E-test, for amphotericin B, caspofungin, itraconazole, voriconazole and posaconazole. *Med. Mycol.* **2012**, *50*, 378–385.
35. Mosmann, T. Rapid colorimetric assay for cellular growth and survival: Application to proliferation and cytotoxicity assays. *J. Immunol. Method.* **1983**, *65*, 55–63. [[CrossRef](#)] [[PubMed](#)]
36. Mourougou-Candoni, N.; Prunet-Foch, B.; Legay, F.; Vignes-Adler, M.; Wong, K. Influence of dynamic surface tension on the spreading of surfactant solution droplets impacting onto a low-surface-energy solid substrate. *J. Colloid. Interface Sci.* **1997**, *192*, 129–141. [[CrossRef](#)]
37. Malkin, A.I. Regularities and mechanisms of the Reh binder's effect. *Colloid J.* **2012**, *74*, 223–238. [[CrossRef](#)]
38. Turganbay, S.; Aidarova, S.; Kumargaliyeva, S.; Argimbayev, D.; Sabitov, A.; Iskakbayeva, Z.; Lyu, M. Mechanochemical synthesis of hydrophilic sulfur nanoparticles in aqueous surfactant solutions and their antibacterial activity and acute toxicity in mice. *ES Mater. Manuf.* **2024**, *23*, 1020. [[CrossRef](#)]
39. Park, H.M.; Lee, W.M. Helmholtz–Smoluchowski velocity for viscoelastic electroosmotic flows. *J. Colloid Interfac. Sci.* **2008**, *317*, 631–636. [[CrossRef](#)]
40. Polaczyk, A.L.; Amburgey, J.E.; Alansari, A.; Poler, J.C.; Propato, M.; Hill, V.R. Calculation and uncertainty of zeta potentials of microorganisms in a 1:1 electrolyte with a conductivity similar to surface water. *Colloid. Surf. A Physicochem. Eng. Asp.* **2019**, *586*, 124097. [[CrossRef](#)]
41. Suryavanshi, P.; Pandit, R.; Gade, A.; Derita, M.; Zachino, S.; Rai, M. *Colletotrichum* sp.—Mediated synthesis of sulphur and aluminium oxide nanoparticles and its in vitro activity against selected food-borne pathogens. *LWT-Food Sci. Technol.* **2017**, *81*, 188–194. [[CrossRef](#)]
42. Shankar, S.; Pangeni, R.; Park, J.W.; Rhim, J.W. Preparation of sulfur nanoparticles and their antibacterial activity and cytotoxic effect. *Mater. Sci. Eng. C* **2018**, *92*, 508–517. [[CrossRef](#)]
43. Gehlot, P.S.; Kulshrestha, A.; Bharmoria, P.; Damarla, K.; Chokshi, K.; Kumar, A. Surface-active ionic liquid cholinium dodecylbenzenesulfonate: Self-assembling behavior and interaction with cellulose. *ACS Omega* **2017**, *2*, 7451–7460. [[CrossRef](#)] [[PubMed](#)]
44. Purohit, V.B.; Pięta, M.; Pietrasik, J.; Plummer, C.M. Recent advances in the ring-opening polymerization of sulfur-containing monomers. *Polym. Chem.* **2022**, *13*, 4858–4878. [[CrossRef](#)]
45. Ni, X.; Li, Z.; Wang, Y. Adsorption Characteristics of Anionic Surfactant Sodium Dodecylbenzene Sulfonate on the Surface of Montmorillonite Minerals. *Front. Chem.* **2018**, *2*, 390. [[CrossRef](#)] [[PubMed](#)]
46. Zhang, J.; Xu, L.; Wang, S.; Jiang, F. Effect of surfactant on the preparation of sulfur nanoparticles via a liquid-phase process. *J. Nanopart. Res.* **2015**, *17*, 338.
47. Parmar, K.; Murthy, Z. CTAB-assisted synthesis of uniform ZnS nanoparticles: Investigation on phase, crystallinity, and optical properties. *J. Cryst. Growth* **2013**, *373*, 1–7.
48. Mahmoodi, N.M.; Abdi, J.; Bastani, D. Direct dyes removal using modified magnetic ferrite nanoparticle. *Iran. J. Environ. Health Sci. Eng.* **2014**, *12*, 96. [[CrossRef](#)]
49. Zhang, F.; He, Z.; Luo, X.; Zhang, S. Preparation and characterization of NaCMC stabilized ZnO nanoparticles. *Colloid. Surf. B Biointerfac.* **2010**, *76*, 520–526. [[CrossRef](#)]
50. Hua, C.; Wang, H.; Jiang, G. Antibacterial nanocomposites based on PHMG-modified nanofibrillated cellulose: Synthesis, characterization, and application. *Cellulose* **2020**, *27*, 3835–3847.
51. Dop, R.A.; Neill, D.R.; Hasell, T. Sulfur-Polymer Nanoparticles: Preparation and Antibacterial Activity. *ACS Appl. Mater. Interfac.* **2023**, *15*, 20822–20832. [[CrossRef](#)]
52. Suleiman, M.; Al-Masri, M.; Al Ali, A.; Aref, D.; Hussein, A.; Saadeddin, I.; Warad, I. Synthesis of Nano-sized Sulfur Nanoparticles and their Antibacterial Activities. *J. Mater. Environ. Sci.* **2015**, *6*, 513–518. Available online: [https://www.jmaterenvirosci.com/Document/vol6/vol6\\_N2/60-JMES-1108-2014-Suleiman.pdf](https://www.jmaterenvirosci.com/Document/vol6/vol6_N2/60-JMES-1108-2014-Suleiman.pdf) (accessed on 10 June 2024).

**Disclaimer/Publisher's Note:** The statements, opinions and data contained in all publications are solely those of the individual author(s) and contributor(s) and not of MDPI and/or the editor(s). MDPI and/or the editor(s) disclaim responsibility for any injury to people or property resulting from any ideas, methods, instructions or products referred to in the content.